⌘ *Author's Choice*

THE JOURNAL OF BIOLOGICAL CHEMISTRY VOL. 286, NO. 17, pp. 15535–15542, April 29, 2011

Molecular Mechanism Underlying Phosphatidylinositol 4,5-Bisphosphate-induced Inhibition of SpIH Channels*

Received for publication, December 20, 2010, and in revised form, February 15, 2011 Published, JBC Papers in Press, March 7, 2011, DOI 10.1074/jbc.M110.214650

Galen E. Flynn and William N. Zagotta[1]

From the Department of Physiology and Biophysics, Howard Hughes Medical Institute, University of Washington, Seattle, Washington 98195-7290

Many ion channels have been shown to be regulated by the membrane signaling phospholipid phosphatidylinositol 4,5-bisphosphate (PIP_2). Here, we demonstrate that the binding of PIP_2 to SpIH, a sea urchin hyperpolarization-activated cyclic nucleotide-gated ion channel (HCN), has a dual effect: potentiation and inhibition. The potentiation is observed as a shift in the voltage dependence of activation to more depolarized voltages. The inhibition is observed as a reduction in the currents elicited by the partial agonist cGMP. These two effects were separable and arose from PIP_2 binding to two different regions. Deletion of the C-terminal region of SpIH removed PIP_2-induced inhibition but not the PIP_2-induced shift in voltage dependence. Mutating key positively charged amino acids in the C-terminal region adjacent to the membrane selectively disrupted PIP_2-induced inhibition, suggesting a direct interaction between PIP_2 in the membrane and amino acids in the C-terminal region that stabilizes the closed state relative to the open state in HCN channels.

HCN channels are integral membrane proteins that are activated by membrane hyperpolarization and modulated by the direct binding of intracellular cyclic nucleotides. These channels underlie the I_f current in cardiac cells, where they tune pacemaker activity, and the I_h current in neuronal cells, where they act to oppose deviations away from the resting membrane potential, thereby stabilizing cellular excitability (1–8). There are four mammalian isoforms, HCN1–HCN4 (9–11). They are members of the voltage-activated family of ion channel proteins. Like other members of this family, HCN channels are tetramers of similar or identical subunits that surround a central ion-conducting pore through the membrane. Each subunit is composed of a cytoplasmic N- and C-terminal region and a core region formed by the six transmembrane helices S1–S6. A single transmembrane pore is formed by the S5-S6 segments contributed by each of the four subunits, whereas the four voltage-sensing domains are formed by the S1–S4 segments from individual subunits (1–8, 12, 13).

The cytoplasmic C-terminal region contains a cyclic nucleotide-binding domain (CNBD)[2] and a C-linker domain that connects the CNBD to the pore. In most mammalian HCN channels, binding of cAMP to the CNBD results in a depolarizing shift in the voltage dependence of activation, causing these channels to open more easily at resting membrane potentials (14, 15). However, in the HCN channel from sea urchin (SpIH), binding of cAMP does not shift the voltage dependence but causes a large increase in the current due to the removal of autoinhibition (4). The atomic structures of the C-terminal region of both HCN2 and SpIH bound to cAMP have been resolved by x-ray crystallography (Fig. 1) (15, 16). In each case, the C-terminal fragments assemble as 4-fold symmetric tetramers. The C-linker regions of each subunit form a gating ring predicted to be adjacent to the cytoplasmic surface of the membrane (Fig. 1*A*). Attached to each C-linker is the CNBD (Fig. 1*B*). The CNBD of HCN channels shares substantial sequence and structural similarity with the CNBD of other cyclic nucleotide-binding proteins such as cAMP-dependent protein kinase and catabolite gene activator protein (15, 17, 18). Interestingly, despite the functional differences between SpIH and HCN2, their structures are very similar (root mean square deviation of the Cα atoms of 0.86 Å) (15, 16).

Recently, acidic phospholipids were shown to regulate HCN channel activation. Direct application of either exogenous phosphatidylinositol 4,5-bisphosphate (PIP_2) or its soluble form, dioctanoyl (diC_8)-PIP_2, to excised inside-out patches containing HCN channels causes a depolarizing shift in the voltage dependence of activation (19, 20). The PIP_2-induced shift occurs in all mammalian HCN channels tested thus far (HCN1, HCN2, and HCN4). In addition, PIP_2 also shifts the activation voltage of $HCN2_{\Delta CNBD}$ channels, in which the CNBD was deleted, suggesting that the mechanism for the voltage-dependent shift by PIP_2 is distinct from the mechanism for the voltage-dependent shift by cAMP (19).

Here, we show that, in addition to shifting the voltage dependence of activation, PIP_2 also inhibits SpIH channels. Our results suggest that PIP_2 binds to two separate regions: 1) the transmembrane core region, which produces potentiation, and 2) the C-linker domain, which produces inhibition. Two basic residues in the C-linker domain near the membrane were found to be involved in the inhibition of the channel by PIP_2. These results suggest a model in which membrane-incorporated PIP_2

* This work was supported, in whole or in part, by National Institutes of Health Grant EY10329 from NEI (to W. N. Z.). This work was also supported by the Howard Hughes Medical Institute.

⌘ *Author's Choice*—Final version full access.

[1] To whom correspondence should be addressed: Dept. of Physiology and Biophysics, P.O. Box 357290, University of Washington, Seattle, WA 98195-7290. Tel.: 206-685-3878; Fax: 206-543-0934; E-mail: zagotta@u.washington.edu.

[2] The abbreviations used are: CNBD, cyclic nucleotide-binding domain; PIP_2, phosphatidylinositol 4,5-bisphosphate; diC_8, dioctanoyl; PIP, phosphatidylinositol 4-monophosphate; CNG, cyclic nucleotide-gated.

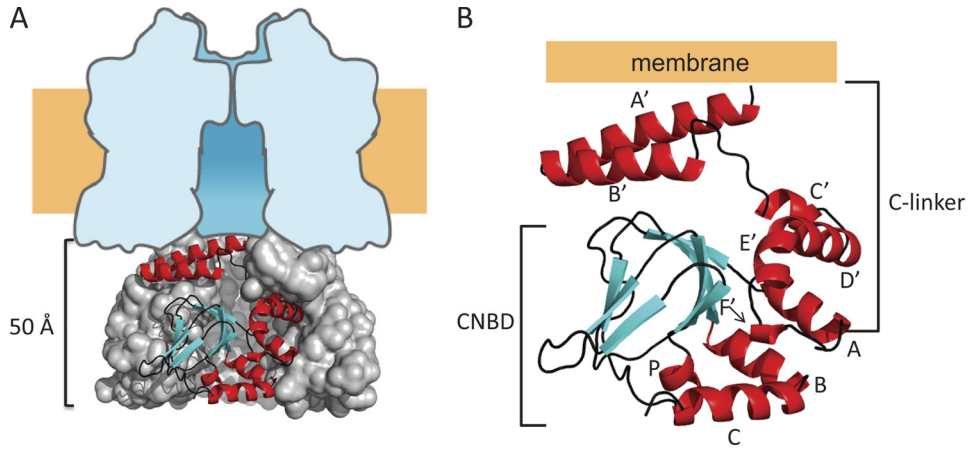

FIGURE 1. **Summary of the structure of a SpIH C-terminal fragment.** *A*, side view showing the SpIH C-terminal structure (amino acids 470–665). Three subunits are shown in a surface representation, and one subunit is in ribbon representation. The tetrameric structure is positioned beneath a schematic diagram representing the transmembrane domain idealized from the space-filled model of Kv1.2 (32). *B*, ribbon representation of a single SpIH C-terminal structure (Protein Data Bank code 2PTM). Helices are colored *red* (A′–F′, A–C, and P), β-sheets are colored *cyan*, and connecting loops are colored *black*.

binds to the C-linker and stabilizes the closed state of the HCN channel.

EXPERIMENTAL PROCEDURES

DNA Preparation for Physiology—SpIH cDNA (a gift from U. B. Kaupp) was subcloned into the pGEMHE high expression vector (a gift from E. Liman), where it was flanked by the *Xenopus* β-globin gene 5′- and 3′-UTRs. All cDNAs were linearized by digestion with SphI and then transcribed *in vitro* using the Ambion T7 mMESSAGE mMACHINE into mRNAs. The mRNA was injected into surgically isolated stage IV *Xenopus* oocytes as described previously (21). All mutations were generated using oligonucleotide-directed PCR mutagenesis and confirmed with fluorescence-based DNA sequencing.

Electrophysiology—Electrophysiology experiments were conducted on full-length and truncated SpIH or SpIH mutant channels exogenously expressed in plasma membranes of *Xenopus* oocytes. SpIH currents were recorded from excised inside-out macropatches using conventional patch-clamp recording techniques (22). Both pipette and bath solutions contained 130 mM KCl, 0.2 mM EDTA, and 3 mM HEPES (pH 7.2). To modulate SpIH and mutant channels, saturating concentrations of cyclic nucleotides (1 mM cGMP or cAMP) were applied in the absence or presence of 10–30 μM PIP_2 using a rapid solution changer (RSC-100, Bio-Logic). Ionic currents were amplified and low pass-filtered at 2 kHz using an Axopatch 200A system (Axon Instruments, Inc.). The currents were digitized at 10 kHz using an ITC-16 DA/AD converter (Instrutech Corp.) interfaced to a computer running PULSE software (HEKA Electronics, Inc.) and stored in files for offline analysis using IGOR software (WaveMetrics) or Excel software (Microsoft).

diC_8-PIP_2 and diC_8-phosphatidylinositol-4-monophosphate (PIP) were purchased from Avanti Polar Lipids and stored at −20 °C until needed. On the day of the experiment, 1.5 mM stock solutions were made by adding water to the newly opened vial unless we were studying dose-response relationships. In that case, we added 1 mM cGMP in recording buffer instead of water. The solution was then kept on ice. Just prior to the application to the patch, the PIP_2 was diluted with 1 mM cGMP to 10 or 30 μM generally in a volume of 2 ml. The solution was applied to the cytoplasmic side of inside-out patches within 3 min using a gravity-controlled perfusion system (RSC-100). Currents in response to voltages from −20 to −120 mV were continuously measured during the application of PIP_2 for 10 min or until we lost the patch.

Data Analysis—To determine the voltage dependence and shifts in voltage dependence due to PIP_2 modulation, we calculated the conductance-voltage (*G-V*) relationship for wild-type and mutant channels in the absence and presence of cyclic nucleotides and cyclic nucleotides + PIP_2. Peak tail current amplitudes were measured at −40 mV after being presented with an activating test pulse voltage given in the range of −20 to −130 mV. Currents were plotted against the test voltages (*G-V* plot), and the data were fit with the Boltzmann equation: $G = \text{base} + G_{\max,\text{cNMP}}/(1 + e(-z\delta(V - V_{1/2})F/RT))$, where base is the non-voltage-dependent leak conductance, V is the test pulse voltage, $V_{1/2}$ is the activation midpoint voltage, and $z\delta$ is the equivalent charge movement. We corrected for leak conductance by subtracting the non-voltage-dependent conductance (base) determined from the Boltzmann fit. The currents were normalized to the $G_{\max,\text{cAMP}}$ determined at saturating voltages, −120 mV or greater. All fitting was performed with IGOR software.

To calculate the energetic effects on SpIH channel opening caused by PIP_2 modulation ($\Delta\Delta G$), we assumed that our mutations outside the cyclic nucleotide-binding site did not change the cyclic nucleotide specificity of the channel. Therefore, the ratio of the opening equilibrium constants for cAMP and cGMP will be constant for all wild-type and mutant channels. Using the published values for wild-type SpIH channel open probability in cAMP ($P_{o,\text{cAMP}} = 0.91$) and cGMP ($P_{o,\text{cGMP}} = 0.54$) (16), we calculated the opening equilibrium constants (L_{cAMP} and L_{cGMP}) for wild-type SpIH channels: $L_{\text{cGMP}} = P_{o,\text{cGMP}}/(1 - P_{o,\text{cGMP}})$ and $L_{\text{cAMP}} = P_{o,\text{cAMP}}/(1 - P_{o,\text{cAMP}})$). Using these L values, we calculated the maximum conductance ($G_{\max}$) from G_{cAMP} and G_{cGMP} measured in each experiment

using the following equation: $G_{max} = ((L_{cGMP}/L_{cAMP}) - 1)/(((L_{cGMP}/L_{cAMP})/G_{cGMP}) - (1/G_{cAMP}))$. With G_{max}, we determined the energetics of channel opening using $\Delta G = -RT \ln((G/G_{max})/(1 - (G/G_{max})))$, where G represents the conductance determined for cAMP, cGMP, or cGMP + PIP_2 at saturating negative voltages; R is the ideal gas constant; and T is the absolute temperature. We also calculated the difference in opening free energy change resulting from PIP_2 binding using the following equation: $\Delta\Delta G = \Delta G_{cGMP,PIP_2} - \Delta G_{cGMP}$.

Data for PIP_2 and PIP dose-response relationships were taken from current measurements at saturating negative test voltages to −120 mV and normalized to $I_{max,No\ PIP}$. Current amplitudes were plotted against applied PIP_2 or PIP concentration, and data were fit with the Hill equation: $I = (I_{base}/(I_{max,No\ PIP_2} - I_{base}))/(1 + (K_{1/2}/[PIP_2])^h)$, where $[PIP_2]$ is the phospholipid concentration, $K_{1/2}$ is the agonist concentration eliciting half-maximal response, and h is the Hill coefficient.

Data parameters were expressed as means ± S.E. and tabulated for comparison. One-way analysis of variance was performed using the Microsoft Excel statistical function with a significance level of 0.05. A post hoc Student's t test was used to determine which of the mutants was statistically different at $p < 0.05$.

RESULTS

Cyclic Nucleotide Regulation of SpIH—HCN channels open their transmembrane pore in response to both membrane hyperpolarization and the direct binding of cyclic nucleotides to a specialized C-terminal domain (1, 2). SpIH is an HCN channel from sea urchin that exhibits properties somewhat different from those of mammalian HCN channels (4). In the absence of cyclic nucleotides, SpIH currents recorded from inside-out macropatches of *Xenopus* oocytes were very small and rapidly inactivated in response to membrane hyperpolarization (Fig. 2*A*, *black traces*). After intracellular cAMP was applied, there was a large increase in current associated with a removal of autoinhibition (Fig. 2*A*, *red trace*) (23, 24). Unlike for mammalian HCN channels, cAMP causes little or no shift in the voltage dependence of SpIH (4). Interestingly, truncated SpIH channels lacking a C-terminal region ($SpIH_{\Delta C}$) produced large non-inactivating currents that were insensitive to cAMP (Fig. 2*B*) (13, 24). The response of $SpIH_{\Delta C}$ channels to membrane hyperpolarization was similar to that of wild-type SpIH channels bound to cAMP. These and similar results in mammalian HCN channels led to the conclusion that, in HCN channels, the C-terminal domain acts as an autoinhibitory domain and that the binding of cyclic nucleotides releases this inhibition, facilitating channel opening (24).

SpIH channels also differ from other HCN channels in agonist specificity (4). As shown in Fig. 2, application of 1 mM cAMP to SpIH channels caused a dramatic increase in the current over control currents in the absence of cyclic nucleotide (Fig. 3, *A* and *B*, *dashed red versus dashed black traces*). Unlike for other HCN channels, however, cGMP behaved as a partial agonist of SpIH channels (Fig. 3, *A* and *B*, *dashed green versus dashed red traces*). At hyperpolarized voltages, saturating concentrations of cGMP activated only about half the amount of current activated by cAMP (16). The difference in the amount

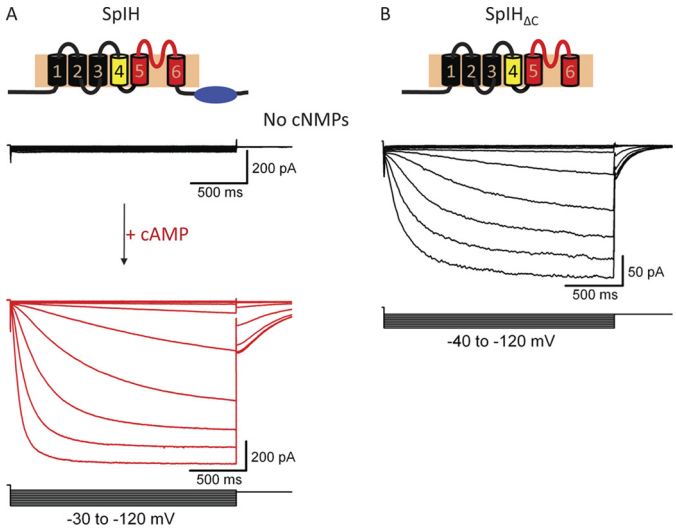

FIGURE 2. **The C terminus acts as an autoinhibitory domain.** *A*, schematic of the membrane topology of a single subunit of the SpIH channel. Representative currents were measured from inside-out excised patches of oocyte membrane. Voltage pulses were applied to patches in the range of −30 to −120 mV, followed by a voltage step to −40 mV. The holding voltage was 0 mV. Currents were measured in the absence of cyclic nucleotides (*black traces*) and in the presence of 1 mM cAMP (*red traces*). *B*, schematic representing the topology of the C-terminal deletion mutant (deleted amino acids 471–767). Representative currents were measured over a voltage range of −40 to −120 mV from a 0-mV holding potential in the absence of cyclic nucleotides.

of current elicited by saturating cGMP and cAMP reflects a difference in efficacy between the two ligands to stabilize the open state of the channel relative to the closed state and not a difference in single-channel conductance (16). These results indicate that, in SpIH channels, cGMP only partially stabilizes channel opening, whereas cAMP produces a greater stabilization. Therefore, the partial activation by cGMP can be used as a sensitive reporter of the energetics of agonist activation of SpIH channels.

PIP_2 Regulation of SpIH—Earlier studies have shown that PIP_2 acts as an allosteric modulator of mammalian HCN channels. Depletion of endogenous PIP_2 from the membrane causes a negative shift in voltage dependence upon patch excision (19, 20). Additionally, when exogenous PIP_2 or the soluble form, diC_8-PIP_2, is applied to HCN channels in inside-out patches, a positive shift in voltage dependence of activation occurs (19). We used the voltage dependence and cyclic nucleotide dependence of gating in SpIH channels to study the molecular mechanism of phosphoinositide modulation using soluble diC_8-PIP_2 (hereafter referred to as PIP_2). We found that, as in mammalian HCN channels, PIP_2 modulated SpIH channels (Fig. 3*A*, *solid traces*). After an initial 20-min waiting period for the depletion of endogenous PIP_2, we applied 10 μM PIP_2 to SpIH channels in inside-out patches, which caused a positive shift in the voltage dependence of activation in the presence of either cAMP or cGMP (Fig. 3*B*, *solid traces*). PIP_2 shifted the midpoint of the activation ($\Delta V_{1/2}$) ~10 mV toward depolarizing voltages for both cAMP and cGMP (Fig. 3*C*).

Interestingly, however, in SpIH, PIP_2 also produced a significant inhibition of the currents measured at hyperpolarized voltages and saturating cGMP concentrations (Fig. 3*A*). In the absence of PIP_2, the maximum conductance of cGMP-modu-

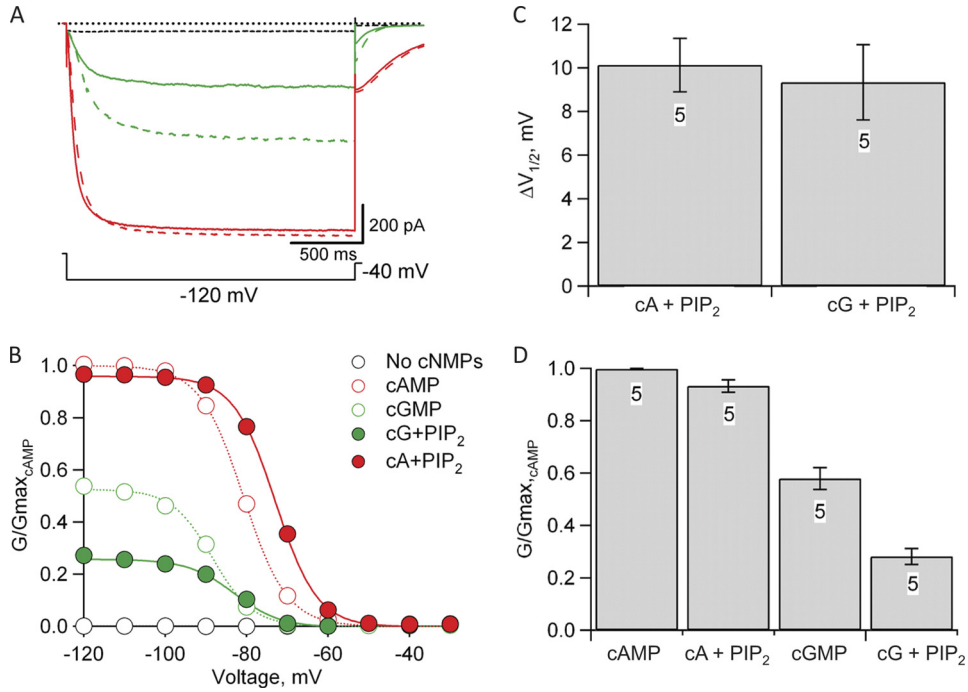

FIGURE 3. **Effects of PIP$_2$ on cyclic nucleotide-modulated SpIH channels.** *A*, representative currents measured in response to a hyperpolarizing voltage step to −120 mV, followed by a voltage step to −40 mV from a holding voltage of 0 mV. Currents were measured in the absence of cyclic nucleotide (*dashed black trace*) and in the presence of 1 mM cGMP (*dashed green trace*), 1 mM cAMP (*dashed red trace*), cAMP + 10 μM diC$_8$-PIP$_2$ (*solid red trace*), and cGMP + 10 μM diC$_8$-PIP$_2$ (*solid green trace*). *B*, normalized *G-V* relationships for each condition in *A*. Tail currents at −40 mV were measured and normalized to the tail currents measured in the presence of 1 mM cAMP (*dashed red trace* in *A*). *Solid* and *dotted curves* represent fits to the data of the Boltzmann equation (see "Experimental Procedures"). Leak currents were subtracted as described under "Experimental Procedures." *C*, bar graph showing the mean ± S.E. of the PIP$_2$-induced shift in the midpoint of the voltage dependence ($\Delta V_{1/2} = V_{1/2,PIP_2} - V_{1/2}$) for both cAMP- and cGMP-modulated channels ($n = 5$). *D*, bar graph showing the mean ± S.E. of the relative normalized conductance ($G/G_{max,cAMP}$) for cyclic nucleotide-modulated channels in the absence and presence of PIP$_2$ ($n = 5$). *cA*, cAMP; *cG*, cGMP.

lated channels was about half the conductance of cAMP-modulated channels ($G_{cGMP}/G_{max,cAMP} = 0.57 \pm 0.04$, $n = 5$) (Fig. 3*B*, *dotted green curve*). Assuming a simple closed-open equilibrium, this fractional activation by cGMP corresponds to a free energy change (ΔG) for opening in cGMP of -0.11 ± 0.09 kcal/mol ($n = 5$) (see "Experimental Procedures"). After 10 min in the presence of 10 μM PIP$_2$, the cGMP-induced current at hyperpolarized voltages was inhibited by ~50% ($G_{cGMP,PIP_2}/G_{max,cAMP} = 0.28 \pm 0.03$, $n = 5$ (Fig. 3*B*, *solid green curve*); or $\Delta G = 0.61 \pm 0.08$ kcal/mol (Fig. 3*D*)). This suggests that PIP$_2$ caused a change in the free energy of opening in the presence of cyclic nucleotides ($\Delta\Delta G$) of ~0.72 ± 0.02 kcal/mol ($n = 5$). As expected for a change in free energy, currents measured in the more efficacious agonist cAMP exhibited a much smaller decrease in 10 μM PIP$_2$ ($G_{cAMP,PIP_2}/G_{max,cAMP} = 0.93 \pm 0.02$, $n = 5$) (Fig. 3*D*). The inhibition seen at large negative voltages at saturating cyclic nucleotide concentrations suggests that PIP$_2$ is stabilizing the closed state of channels relative to the open state.

Localization of PIP$_2$ Effects—We observed that PIP$_2$ produced two effects on SpIH channels: potentiation of the voltage-dependent gating and inhibition of the cyclic nucleotide-dependent gating. To identify regions involved in PIP$_2$ regulation, we applied PIP$_2$ to SpIH$_{\Delta C}$ channels. As shown previously, currents measured from channels lacking a C-terminal region were large and similar in time course to currents measured in the presence of cAMP (Fig. 4*A*). We found that 30 μM PIP$_2$ produced a depolarizing shift in the voltage dependence that changed the half-maximal activating voltage ($\Delta V_{1/2}$) by 4.8 ± 0.9 mV ($n = 3$) (Fig. 4, *B*, *C*, and *G*). This voltage shift for SpIH$_{\Delta C}$ was similar although somewhat smaller than what we observed in wild-type SpIH channels bound by cAMP or cGMP. In contrast to wild-type channels, however, PIP$_2$ did not inhibit SpIH$_{\Delta C}$. On the contrary, SpIH$_{\Delta C}$ exhibited a small reversible potentiation in the maximum conductance ($G_{PIP_2}/G_{max,No\ PIP_2} = 1.13 \pm 0.06$, $n = 3$) (Fig. 4, *C* and *H*), unlike cAMP-modulated wild-type SpIH channels (Fig. 3). Similarly, SpIH channels lacking both N- and C-terminal regions (SpIH$_{\Delta NC}$) also showed a depolarizing shift in voltage dependence ($\Delta V_{1/2} = 7.8 \pm 0.98$ mV, $n = 4$) and a small reversible increase in maximum conductance ($G_{PIP_2}/G_{max,No\ PIP_2} = 1.09 \pm 0.24$, $n = 4$) (Fig. 4, *E–H*). These results show that the potentiating effects of PIP$_2$ on voltage-dependent gating can be physically separated from the inhibitory effects of PIP$_2$ on ligand gating. The reversible increase in maximum conductance observed in the deletion mutants is a further indication that the potentiating effect induced by PIP$_2$ is distinct from the inhibitory effect, which accounts for the lack of an increase in conductance in wild-type SpIH in the presence of cAMP. From these results, we conclude that PIP$_2$ interacts with two distinct sites on the channel: one site in the transmembrane region (amino acids 161–470) that shifts the voltage dependence and a second site in the intracellular C-terminal region (deleted amino acids 471–767) that inhibits the cyclic nucleotide regulation.

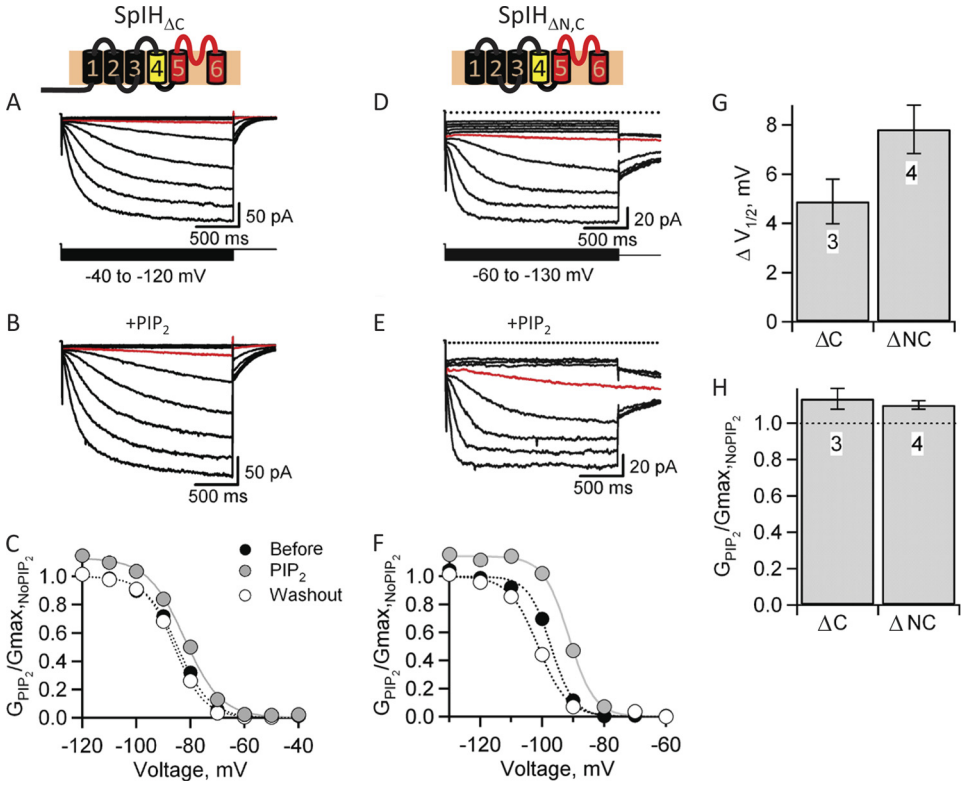

FIGURE 4. **The C-terminal domain mediates PIP$_2$ inhibition and the transmembrane domain mediates PIP$_2$-induced positive shift in voltage.** *A* and *B*, representative currents recorded from SpIH$_{\Delta C}$ channels lacking the C-terminal region (deleted amino acids 471–767) in response to voltage steps between −40 and −130 mV in the absence and presence of 30 μM diC$_8$-PIP$_2$. The *red trace* indicates currents measured at the same voltage, −70 mV. *C*, *G-V* relationships for SpIH$_{\Delta C}$ measured from tail currents at −40 mV in the absence of PIP$_2$ (*black circles*), in the presence of 30 μM diC$_8$-PIP$_2$ (*gray circles*), and after PIP$_2$ was washed out (*white circles*). The curves represent fits of the Boltzmann equation to the data. *D* and *E*, representative currents recorded from C-terminal deleted SpIH$_{\Delta NC}$ channels (deleted amino acids 1–160 and 471–767) in response to voltage steps between −40 and −130 mV in the absence and presence of 30 μM diC$_8$-PIP$_2$. The *red trace* indicates currents measured at the same voltage, −90 mV. *F*, *G-V* relationships for SpIH$_{\Delta NC}$ measured from tail currents at −90 mV in the absence of PIP$_2$ (*black circles*), in the presence of 30 μM diC$_8$-PIP$_2$ (*gray circles*), and after PIP$_2$ was washed out (*white circles*). *G*, change in voltage dependence as determined for the difference in $V_{1/2}$ before and after modulation by PIP$_2$ ($\Delta V_{1/2}$). *H*, normalized conductance in diC$_8$-PIP$_2$ for SpIH$_{\Delta C}$ and SpIH$_{\Delta NC}$.

Identification of the PIP$_2$ Site for Inhibition of Cyclic Nucleotide-dependent Gating—The acyl chains of PIP$_2$ are expected to intercalate into the hydrophobic regions of the plasma membrane, whereas the negatively charged headgroup extends into the cytoplasm. Given this physical arrangement of these molecules, the negative charges on PIP$_2$ most likely interact with positively charged residues in the region of the HCN channel protein adjacent to the membrane. The atomic structure of the C-terminal region of SpIH was resolved by x-ray crystallography (Fig. 1) (16). The C-terminal region contains a C-linker domain followed by a CNBD. The C-linker domain begins immediately after the pore-lining S6 transmembrane helix and contains six α-helices (A′–F′). It is the site of virtually all of the intersubunit interactions in the C-terminal region, primarily interactions between the A′ and B′ helices of one subunit and the C′ and D′ helices of a neighboring subunit. The A′ helix is predicted to lie adjacent to and nearly parallel to the plasma membrane. The amino acid sequence of the A′ helix contains four positively charged residues, Arg-475, Arg-478, Lys-480, and Lys-482 (Fig. 5*A*). With the exception of Lys-480, all of these residues are on the same surface of the A′ helix, and they all point toward the membrane (Fig. 5*B*). Lys-480 points away from the plasma membrane and interacts with the C′ helix of the neighboring subunit through a salt bridge with Glu-522. Arg-475, Arg-478, and Lys-482 are positioned to interact with PIP$_2$ in the inner leaflet of the membrane.

We hypothesized that the positively charged amino acids of the A′ helix are involved in electrostatic interactions with PIP$_2$ in the plasma membrane and that these interactions are responsible for the PIP$_2$-induced inhibition of SpIH. To test our hypothesis, we mutated each of the three residues individually and quantified the inhibitory effects elicited by PIP$_2$. In each case, a positively charged amino acid was replaced with cysteine. To ensure that our mutant channels were free of endogenous PIP$_2$, we waited 20 min after patch excision for the depletion of endogenous PIP$_2$ before applying exogenous PIP$_2$. We started by characterizing each mutant channel over a range of test voltages, −20 to −120 mV, in the absence of cyclic nucleotides, in 1 mM cGMP, and in 1 mM cAMP (Fig. 6). Two of the mutant channels, R475C and R478C, exhibited increases in the fractional activation by cGMP ($G_{cGMP}/G_{max,cAMP}$) at hyperpolarized voltages relative to wild-type SpIH (Fig. 6, *A–D*). In addition, R475C exhibited an increase in fractional activation in the absence of cyclic nucleotide, suggesting that the CNBD does not autoinhibit R475C mutant channels as efficiently as wild-type channels. The voltage dependence of activation for all three mutants was very close to that for wild-type SpIH.

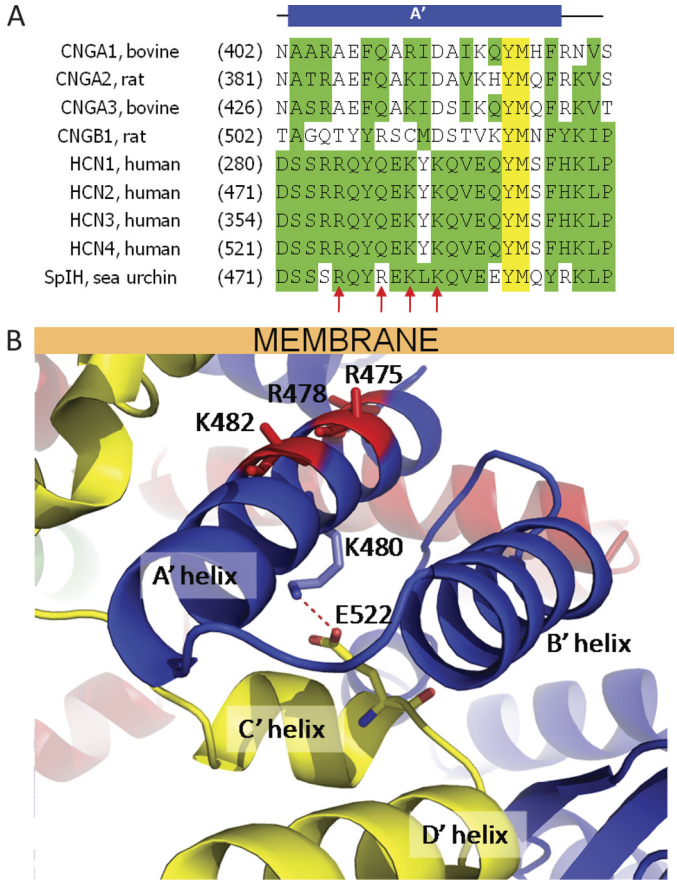

FIGURE 5. **Positively charged residues in the A′ helix of SpIH near the membrane.** *A*, sequence alignment of amino acids in the A′ helix of SpIH and related CNG channels. *Red arrows* indicate the positions of positively charged residues in SpIH. *B*, model of the atomic structure of SpIH showing positive residues in the A′ helix as *sticks* on the ribbon backbone (Lys-475, Arg-478, and Lys-482; *red*). Lys-480 (*blue sticks*) points away from the membrane and forms an intersubunit salt bridge (*dashed red line*) with Glu-522 in the neighboring subunit (*yellow stick* in the *yellow* subunit). The position of the membrane is shown by the *labeled bar*.

Next, we evaluated the functional effects of PIP_2 on each of the three mutant channels. All three mutant channels exhibited depolarizing shifts in voltage in response to 10 μM PIP_2 (Fig. 6, *B*, *D*, and *F*). Although R475C exhibited PIP_2-induced reduction in cGMP-activated current, both R478C and K482C exhibited significantly less inhibition by PIP_2. The amount of PIP_2 inhibition observed depended on the free energy of opening, and for the R475C mutant, the opening in cGMP is more favorable than for the wild type (cGMP is almost a full agonist), so the inhibition appeared less (Fig. 7). Our thermodynamic analysis took this into account (see calculation of ΔG under "Experimental Procedures"). The $\Delta\Delta G$ for PIP_2-induced inhibition of K478C was significantly different from that in the wild type (one-way analysis of variance and post hoc Student's *t* test, $p < 0.01$). These results suggest that Arg-478 and Lys-482 can interact with PIP_2 in the membrane and stabilize the closed state relative to the open state.

Finally, we determined the apparent affinity of PIP_2 and diC_8-PIP for producing inhibition in both wild-type SpIH and the K478C mutant. Currents were recorded in the presence of 1 mM cGMP and varying concentrations of PIP_2 for wild-type SpIH or K478C (Fig. 8, *A* and *B*). The amplitudes of currents elicited by −120-mV test pulses were measured and plotted relative to the PIP_2 concentration (Fig. 8*C*). We averaged the dose-response data from three patches and fit these data with the Hill equation (see "Experimental Procedures"). The fit to the dose-response data for SpIH yielded a maximum inhibition by PIP_2 of $I_{PIP_2}/I_{cGMP,No\ PIP_2} = 55\%$, $K_{1/2} = 3.6$ μM, and Hill coefficient = 1 (Fig. 8*C*, *closed circles*). The maximum inhibition of wild-type SpIH by PIP was $I_{PIP}/I_{cGMP,No\ PIP} = 49\%$, $K_{1/2} = 13.6$ μM, and Hill coefficient = 1 (Fig. 8*D*, *open circles*). In contrast, the dose-response relationships of R478C for both PIP_2 and PIP were nearly flat with respect to the concentration of phosphoinositides (Fig. 8, *C* and *D*, *squares*). These results show that both PIP_2 and PIP inhibit SpIH similarly but with

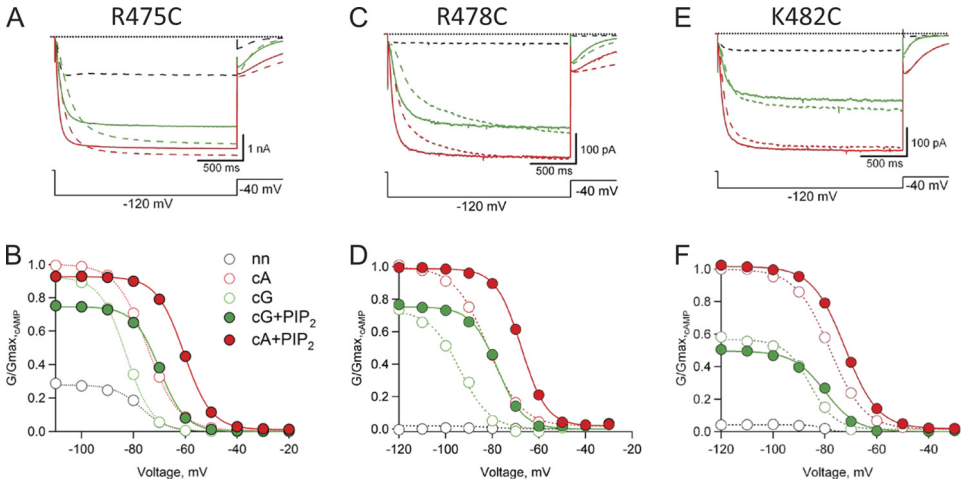

FIGURE 6. **Effects of 10 μM PIP_2 on cyclic nucleotide modulation of mutant SpIH channels (R475C, R478C, and K482C).** *A*, *C*, and *E*, representative currents measured in response to a hyperpolarizing voltage step to −120 mV, followed by a voltage step to −40 mV from a holding voltage of 0 mV. Currents were measured in the absence of cyclic nucleotide (*dashed black trace*) and in the presence of 1 mM cGMP (*dashed green trace*), 1 mM cAMP (*dashed red trace*), cAMP + 10 μM diC_8-PIP_2 (*solid red trace*), and cGMP + 10 μM diC_8-PIP_2 (*solid green trace*). *B*, *D*, and *F*, normalized *G-V* relationships for each mutant. All currents were measured from tail currents at −40 mV and normalized (see "Experimental Procedures"). Data in the absence of PIP_2 are shown as *open circles*, and those in the presence of PIP_2 are shown as *closed circles* (see legend in *B*). *Solid* and *dotted curves* represent fits to the data of the Boltzmann equation (see "Experimental Procedures"). *nn*, no nucleotide; *cA*, cAMP; *cG*, cGMP.

different apparent affinities and that the inhibitory effects are disrupted by the R478C mutation.

DISCUSSION

In this work, we found that PIP_2 had two different and separable effects on SpIH channels. First, as reported previously for mammalian HCN channels (19, 20, 25), PIP_2 potentiated SpIH by causing a depolarizing shift in voltage-dependent activation. Second, PIP_2 also inhibited SpIH, causing a decrease in saturating cGMP-activated currents at maximum hyperpolarizing voltages. For SpIH channels, the inhibition was appreciable only with cGMP and not with cAMP because cGMP is a partial agonist and does not maximally open SpIH channels even at saturating concentrations. As a result of these two different actions of PIP_2, there is a characteristic crossover of the *G-V* relationships, with PIP_2 causing potentiation at depolarized voltages and inhibition at hyperpolarized voltages.

The PIP_2-induced potentiation was localized to the transmembrane region of the channel containing the pore and voltage-sensing domains because PIP_2 produced shifts in the voltage dependence of $SpIH_{\Delta C}$ and $SpIH_{\Delta NC}$. A depolarizing shift in voltage dependence could result from a mechanism in which PIP_2 stabilized either 1) the open state of the pore (relative to the closed state) or 2) the activated (down) state of the voltage sensor (relative to the resting state). These mechanisms can be distinguished based on the effects of PIP_2 on the C-terminal deletion mutants at large hyperpolarizing voltages, where presumably all of the voltage sensors are activated. A stabilization of the open state of the pore might be expected to increase the current even after all the voltage sensors are activated (assuming that the open probability is not already near one). As shown in Fig. 4*G*, PIP_2 caused a small but significant increase in the cGMP-activated current at hyperpolarized voltages in the deletion mutants, suggesting that the potentiating effect of PIP_2 cannot simply be just on the movement of the voltage sensor. However, if all of the potentiating and inhibitory effects of PIP_2 were acting on the pore in wild-type channels, we would not observe the crossover of the *G-V* curves, which is characteristic of the effects of PIP_2 on wild-type SpIH channels. For these reasons, we favor the idea that PIP_2-induced potentiation of voltage-dependent activation arises in part from a stabilization of the activated state of the voltage sensor. Such stabilization could result from a generalized effect of PIP_2 on the potential

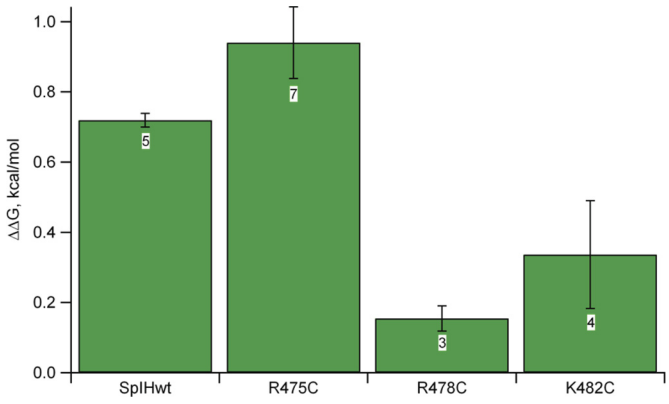

FIGURE 7. **Change in free energy of opening caused by PIP_2 modulation of cGMP-modulated SpIH and mutant channels.** The bar graph represents mean $\Delta\Delta G$ values ± S.E. (see "Experimental Procedures"). Data sample sizes are shown inside *boxes*.

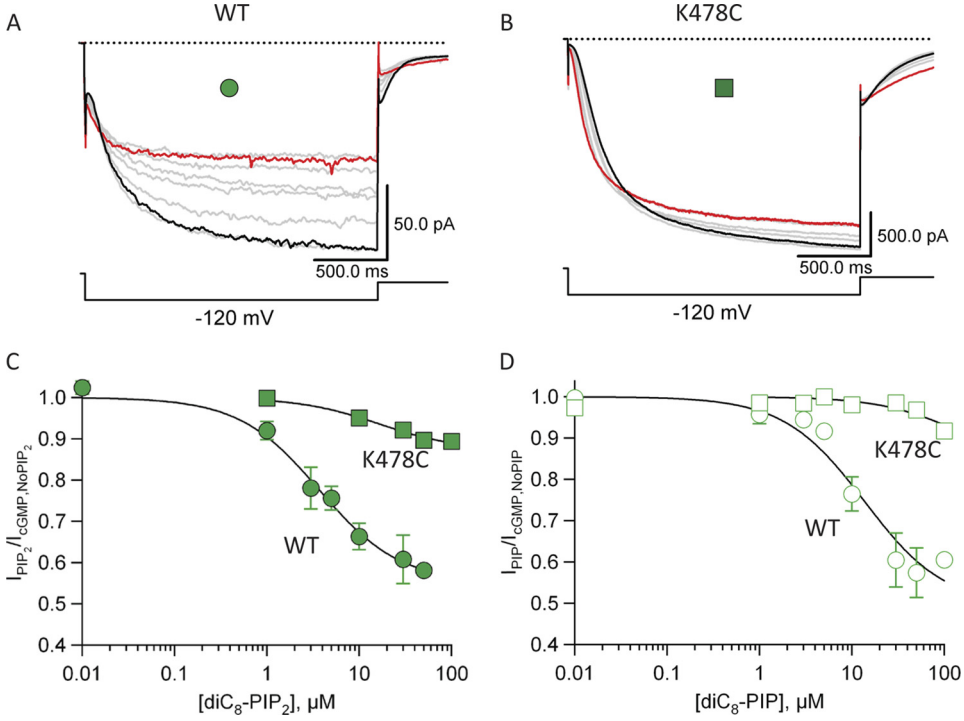

FIGURE 8. **Dose-response relationship of PIP_2 and PIP in SpIH and K478C mutant channels.** *A*, representative SpIH currents measured during a −120-mV test pulse in the presence of 1 mM cGMP (*black trace*) and increasing concentrations of diC$_8$-PIP$_2$ (100 μM = *red trace*). *B*, representative K478C currents measured during a −120-mV test pulse in the presence of 1 mM cGMP (*black trace*) and increasing concentrations of diC$_8$-PIP$_2$ (100 μM = *red trace*). *C* and *D*, data from three patches were averaged and plotted as a function of PIP_2 or PIP concentration, respectively. Data were fit with the Hill equation (see "Experimental Procedures"). For SpIH, $I_{PIP_2}/I_{cGMP,No\ PIP_2}$ = 55%, $K_{1/2,PIP_2}$ = 3.6 μM, $I_{PIP}/I_{cGMP,No\ PIP}$ = 49%, and $K_{1/2,PIP}$ = 13.6 μM.

felt by the voltage sensor (such as a surface charge effect). Alternatively, it could result from a specific electrostatic interaction between the negatively charged PIP_2 and positively charged residues in the activated (down) state of the voltage sensor.

The PIP_2-induced inhibition was localized to the C-terminal region of the channel containing the C-linker and CNBD. Previously, it was proposed that the apo-state of the C-terminal region in HCN channels produces an autoinhibition on channel opening and that the binding of cyclic nucleotide relieves this autoinhibition (24). Consistent with this mechanism, we and others have shown that deletion of the C-terminal region in SpIH channels removes the autoinhibition seen in wild-type SpIH in the absence of cyclic nucleotide (Fig. 2) (13, 24). These results suggest that the mechanism for PIP_2-induced inhibition might be to stabilize the autoinhibitory state of the C-terminal region. The partial agonist cGMP is therefore less able to promote opening in the presence of PIP_2, causing a reduction in current at strong hyperpolarized voltages. However, the full agonist cAMP contributes a greater energy to channel opening and can overcome the inhibition by PIP_2.

A mechanism for autoinhibition has been proposed to involve the C-linker domain (2, 24, 26, 27). The C-linker domain has extensive intersubunit interactions, primarily involving interactions between the A′ and B′ helices of one subunit and the C′ and D′ helices of a neighboring subunit. These helices form a gating ring at the intracellular entrance to the pore that may restrict movement of the S6 region and channel opening. We have shown that mutating Arg-478 and Lys-482, positively charged residues on the A′ helix adjacent to the membrane, disrupts PIP_2-induced inhibition of SpIH. Interestingly, Arg-478 is not conserved among HCN channels, possibly explaining why no consistent inhibition was seen for mammalian HCN2 (see supplemental Fig. S2 in Ref. 19). Therefore, an electrostatic interaction between Arg-478 and Lys-482 with PIP_2 in the inner leaflet of the membrane may help stabilize the gating ring, producing autoinhibition.

PIP_2 has been shown to regulate many other plasma membrane ion channels and transporters. The list includes inwardly rectifying K^+ (Kir) channels, KCNQ channels, transient receptor potential channels, voltage-gated calcium channels, epithelial sodium channels, two-P domain potassium channels (K2p), and ion transporters such as the Na^+-Ca^{2+} exchanger (28, 29). In general, these proteins are activated by PIP_2 or require PIP_2 to function (27). Interestingly, PIP_2 does not activate cyclic nucleotide-gated (CNG) channels. Instead, CNG channels, particularly heteromeric channels formed from CNGA1 and CNGB1 subunits, are inhibited by PIP_2 (30). CNG channels are members of the same cyclic nucleotide-regulated family of channels as HCN channels and contain a C-linker and CNBD structurally similar to the HCN C-terminal region (2, 26, 27). The A′ helix of the CNGB subunit contains a positively charged residue at a site equivalent to Arg-478, and the A′ helix of the CNGA subunit contains a number of positively charged residues at other sites (Fig. 5*A*). As in SpIH, PIP_2 has a dual effect on HERG channels, another member of the cyclic nucleotide-regulated family of channels. Application of PIP_2 to HERG channels shifts the voltage dependence of activation to more negative potentials while it also decreases the rate of inactivation (31). It remains to be determined whether the molecular mechanism for PIP_2 regulation is similar between HCN, CNG, and HERG channels.

Acknowledgments—We are grateful to Kevin Black, Shellee Cunnington, Gay Sheridan, and Stacey Simmons for technical assistance. We thank Drs. Bjoern Falkenburger and Michael Puljung for comments on this manuscript and all members of our local lipid discussion group for helpful suggestions.

REFERENCES

1. Biel, M., Wahl-Schott, C., Michalakis, S., and Zong, X. (2009) *Physiol. Rev.* **89,** 847–885
2. Craven, K. B., and Zagotta, W. N. (2006) *Annu. Rev. Physiol.* **68,** 375–401
3. DiFrancesco, D. (2006) *Prog. Biophys. Mol. Biol.* **90,** 13–25
4. Gauss, R., Seifert, R., and Kaupp, U. B. (1998) *Nature* **393,** 583–587
5. Ludwig, A., Zong, X., Hofmann, F., and Biel, M. (1999) *Cell Physiol. Biochem.* **9,** 179–186
6. Robinson, R. B., and Siegelbaum, S. A. (2003) *Annu. Rev. Physiol.* **65,** 453–480
7. Santoro, B., and Tibbs, G. R. (1999) *Ann. N.Y. Acad. Sci.* **868,** 741–764
8. Wahl-Schott, C., and Biel, M. (2009) *Cell. Mol. Life Sci.* **66,** 470–494
9. Ludwig, A., Zong, X., Jeglitsch, M., Hofmann, F., and Biel, M. (1998) *Nature* **393,** 587–591
10. Santoro, B., Grant, S. G., Bartsch, D., and Kandel, E. R. (1997) *Proc. Natl. Acad. Sci. U.S.A.* **94,** 14815–14820
11. Santoro, B., Liu, D. T., Yao, H., Bartsch, D., Kandel, E. R., Siegelbaum, S. A., and Tibbs, G. R. (1998) *Cell* **93,** 717–729
12. Männikkö, R., Elinder, F., and Larsson, H. P. (2002) *Nature* **419,** 837–841
13. Vemana, S., Pandey, S., and Larsson, H. P. (2004) *J. Gen. Physiol.* **123,** 21–32
14. Viscomi, C., Altomare, C., Bucchi, A., Camatini, E., Baruscotti, M., Moroni, A., and DiFrancesco, D. (2001) *J. Biol. Chem.* **276,** 29930–29934
15. Zagotta, W. N., Olivier, N. B., Black, K. D., Young, E. C., Olson, R., and Gouaux, E. (2003) *Nature* **425,** 200–205
16. Flynn, G. E., Black, K. D., Islas, L. D., Sankaran, B., and Zagotta, W. N. (2007) *Structure* **15,** 671–682
17. Kornev, A. P., Taylor, S. S., and Ten Eyck, L. F. (2008) *PLoS Comput. Biol.* **4,** e1000056
18. Berman, H. M., Ten Eyck, L. F., Goodsell, D. S., Haste, N. M., Kornev, A., and Taylor, S. S. (2005) *Proc. Natl. Acad. Sci. U.S.A.* **102,** 45–50
19. Pian, P., Bucchi, A., Robinson, R. B., and Siegelbaum, S. A. (2006) *J. Gen. Physiol.* **128,** 593–604
20. Zolles, G., Klöcker, N., Wenzel, D., Weisser-Thomas, J., Fleischmann, B. K., Roeper, J., and Fakler, B. (2006) *Neuron* **52,** 1027–1036
21. Zagotta, W. N., Hoshi, T., and Aldrich, R. W. (1989) *Proc. Natl. Acad. Sci. U.S.A.* **86,** 7243–7247
22. Hamill, O. P., Marty, A., Neher, E., Sakmann, B., and Sigworth, F. J. (1981) *Pflugers Arch.* **391,** 85–100
23. Shin, K. S., Maertens, C., Proenza, C., Rothberg, B. S., and Yellen, G. (2004) *Neuron* **41,** 737–744
24. Wainger, B. J., DeGennaro, M., Santoro, B., Siegelbaum, S. A., and Tibbs, G. R. (2001) *Nature* **411,** 805–810
25. Pian, P., Bucchi, A., Decostanzo, A., Robinson, R. B., and Siegelbaum, S. A. (2007) *Pflugers Arch.* **455,** 125–145
26. Craven, K. B., Olivier, N. B., and Zagotta, W. N. (2008) *J. Biol. Chem.* **283,** 14728–14738
27. Craven, K. B., and Zagotta, W. N. (2004) *J. Gen. Physiol.* **124,** 663–677
28. Suh, B. C., and Hille, B. (2005) *Curr. Opin. Neurobiol.* **15,** 370–378
29. Suh, B. C., and Hille, B. (2008) *Annu. Rev. Biophys.* **37,** 175–195
30. Womack, K. B., Gordon, S. E., He, F., Wensel, T. G., Lu, C. C., and Hilgemann, D. W. (2000) *J. Neurosci.* **20,** 2792–2799
31. Bian, J. S., and McDonald, T. V. (2007) *Pflugers Arch.* **455,** 105–113
32. Long, S. B., Campbell, E. B., and Mackinnon, R. (2005) *Science* **309,** 897–903